Effective action, magnetic excitations, and quantum fluctuations in lightly doped single-layer cuprates

Alexander I. Milstein[1] and Oleg P. Sushkov[2]
[1]*Budker Institute of Nuclear Physics, 630090 Novosibirsk, Russia*
[2]*School of Physics, University of New South Wales, Sydney 2052, Australia*

(Received 9 December 2007; revised manuscript received 21 March 2008; published 1 July 2008)

We consider the extended two-dimensional t-t'-t''-J model at zero temperature. Parameters of the model corresponds to doping by holes. Using the low doping effective action, we demonstrate that the system can: (1) preserve the long-range collinear antiferromagnetic order, (2) lead to a spin spiral state (static or dynamic), and (3) lead to the phase-separation instability. We show that at parameters of the effective action corresponding to the single-layer cuprate $La_{2-x}Sr_xCuO_4$, the spin spiral ground state is realized. We derive properties of magnetic excitations and calculate quantum fluctuations. Quantum fluctuations destroy the static spin spiral at the critical doping $x_c \approx 0.11$. This is the point of the quantum phase transition to the spin-liquid state (dynamic spin spiral). The state is still double degenerate with respect to the direction of the dynamic spiral, so this is a "directional nematic." The superconducting pairing exists throughout the phase diagram and is not sensitive to the quantum phase transition. We also compare the calculated neutron-scattering spectra with experimental data.

DOI: 10.1103/PhysRevB.78.014501 PACS number(s): 74.72.Dn, 75.10.Jm, 75.50.Ee

I. INTRODUCTION

The phase diagram of the prototypical cuprate superconductor $La_{2-x}Sr_xCuO_4$ (LSCO) shows that the magnetic state changes tremendously with Sr doping. The three-dimensional antiferromagnetic (AF) Néel order identified[1] below 325 K in the parent compound disappears at doping $x \approx 0.02$ and gives way to the so-called spin-glass phase which extends up to $x \approx 0.055$. In both the Néel and the spin-glass phase, the system essentially behaves as an Anderson insulator and exhibits only hopping conductivity. Superconductivity then sets in for doping $x \gtrsim 0.055$, see Ref. 2. One of the most intriguing properties of LSCO is the static incommensurate magnetic ordering observed at low temperature in *elastic* neutron-scattering experiments. This ordering manifests itself as a scattering peak shifted with respect to the antiferromagnetic position. Very importantly, the incommensurate ordering is a generic feature of LSCO. According to experiments in the Néel phase, the incommensurability is almost doping independent and directed along the orthorhombic b axis.[3] In the spin-glass phase, the shift is also directed along the b axis, but scales linearly with doping.[4–6] Finally, in the underdoped superconducting region ($0.055 \lesssim x \lesssim 0.12$), the shift still scales linearly with doping, but it is directed along the crystal axes of the tetragonal lattice.[7] Very recent studies also reveal the evolution of inelastic neutron spectra with doping.[8]

Near $x=0.12$, certain La-based materials develop a strongly enhanced static incommensurate magnetic order accompanied by small lattice deformation at the second-order harmonics,[9–11] see also Ref. 12 for a review.

Incommensurate features have also been observed in inelastic neutron scattering from $YBa_2Cu_3O_{6+y}$ (YBCO).[13–19] In underdoped YBCO, there is a rather large uncertainty in the determining of the doping level. However, it seems that the incommensurability in YBCO is about 30%–40% smaller than that in LSCO, comparing the same doping level. In a very recent work,[20] the electronic liquid crystal state in underdoped YBCO has been reported. The state has no static spins, but nevertheless, it demonstrates a degeneracy with respect to the direction of the dynamic spin structure. In addition, there are indications that the electronic liquid crystal state observed in Ref. 20 is very close to a quantum phase transition to a state with static spins.

The two-dimensional (2D) t-J model was suggested two decades ago to describe the essential low-energy physics of high-T_c cuprates.[21–23] In its extended version, this model includes additional hopping matrix elements t' and t'' to second- and third-nearest Cu neighbors. The Hamiltonian of the t-t'-t''-J model on the square Cu lattice has the form:

$$H = -t \sum_{\langle ij \rangle \sigma} c_{i\sigma}^{\dagger} c_{j\sigma} - t' \sum_{\langle ij' \rangle \sigma} c_{i\sigma}^{\dagger} c_{j'\sigma} - t'' \sum_{\langle ij'' \rangle \sigma} c_{i\sigma}^{\dagger} c_{j''\sigma} + J \sum_{\langle ij \rangle \sigma} \left(\mathbf{S}_i \mathbf{S}_j - \frac{1}{4} N_i N_j \right). \quad (1)$$

Here, $c_{i\sigma}^{\dagger}$ is the creation operator for an electron with spin σ ($\sigma = \uparrow, \downarrow$) at site i of the square lattice, $\langle ij \rangle$ indicates first-, $\langle ij' \rangle$ second-, and $\langle ij'' \rangle$ third-nearest-neighbor sites. The spin operator is $\mathbf{S}_i = \frac{1}{2} c_{i\alpha}^{\dagger} \sigma_{\alpha\beta} c_{i\beta}$, and $N_i = \Sigma_\sigma c_{i\sigma}^{\dagger} c_{i\sigma}$ with $\langle N_i \rangle = 1 - x$ being the number density operator. In addition to Hamiltonian (1), there is the constraint of no double occupancy, which accounts for strong electron correlations. The values of the parameters of Hamiltonian (1) for LSCO are known from neutron scattering,[1] Raman spectroscopy,[24] and *ab initio* calculations.[25] The values are: $J \approx 140$ meV, $t \approx 450$ meV, $t' \approx -70$ meV, and $t'' \approx 35$ meV. Hereafter, we set $J=1$, hence we measure energies in units of J.

The idea of spin spirals in the t-J model at finite doping was first suggested in Ref. 26. The idea had initially attracted a lot of attention, see e.g., Refs. 27–30. However, it has been soon realized that there was a fundamental unresolved theoretical problem of stability of the spiral.[30] Together with lack

 ©2008 The American Physical Society

of experimental confirmations, this was a very discouraging development. The observation of static and quasistatic incommensurate peaks in neutron scattering caused a renewal of theoretical interest in the idea of spin spirals in cuprates.[31–39] It has been realized that in LSCO, the charge disorder related to a random distribution of Sr ions plays a crucial role and in the insulating state, $x \leq 0.055$, the disorder qualitatively influences the problem of stability of the spiral. The point is that in the insulating state, the mobile holes are not really mobile, they are trapped in shallow hydrogenlike bound states near Sr ions. The trapping leads to the diagonal spin spiral.[34,37–39] Percolation of the bound states gives way to superconductivity, and in the percolated state, the spin spiral must be directed along crystal axes of the tetragonal lattice.[34] So the percolation concentration is $x_{\text{per}}=0.055$. The rotation of the direction of the spin spiral is dictated by the Pauli exclusion principle. The disorder at $x>0.055$ is still pretty strong. However, unlike in the insulating phase, the disorder does not play a qualitative role and therefore in the first approximation, one can disregard it. Thus, we arrive at the case of small uniform doping. This is the problem we address in the present work.

As we already mentioned, the case of an uniform spin spiral (no external disorder) in a doped quantum antiferromagnet has an inherent theoretical problem. If considered in the semiclassical approximation, the out-of-plane magnon is marginal and in the end this implies an instability of the spin spiral.[30] An attempt to fix the problem by account of quantum fluctuations within the $1/S$ spin-wave theory was done in Ref. 32. We understand now that, while being qualitatively correct, the work[32] did not account for all relevant quantum fluctuations. The effective action method is much more powerful than the $1/S$ expansion because the method accounts for all symmetries exactly and generates a regular expansion in powers of doping x, this is the true chiral perturbation theory. This is why, in the present work, we employ the effective action method.

The structure of the paper is the following. In Sec. II, we discuss the effective low-energy action of the modified t-J model. Section III addresses the issue of stability of the Néel state under doping. The spiral ground state in the mean-field approximation is considered in Sec. IV. The in-plane magnons are discussed in Sec. V and out-of-plane magnons in Sec. VI. Section VII addresses the quantum fluctuations and the quantum phase transition to the directional nematic. Finally, discussion and comparison with experiments is presented in the Sec. VIII.

II. EFFECTIVE LOW-ENERGY ACTION OF 2D t-t'-t''-J MODEL AT SMALL DOPING

At zero doping (no holes), the t-J model is equivalent to the Heisenberg model and describes the Mott insulator La_2CuO_4. The removal of a single electron from this Mott insulator, or in other words the injection of a hole, allows the charge carrier to propagate. Single-hole properties of the t-J model are well understood, see Ref. 41 for a review. A calculation of the hole dispersion at values of parameters t, t', and t'' corresponding to the single-layer cuprate LSCO has been performed in Ref. 32 using the self-consistent born approximation (SCBA), see also Ref. 37. According to this calculation, the dispersion of the hole dressed by magnetic quantum fluctuations has minima at the nodal points $\mathbf{q}_0 = (\pm\pi/2, \pm\pi/2)$, and it is practically isotropic in the vicinity of each point,

$$\epsilon(\mathbf{p}) \approx \frac{1}{2}\beta\mathbf{p}^2, \tag{2}$$

where $\mathbf{p}=\mathbf{q}-\mathbf{q}_0$. We set the lattice spacing to unity, 3.81 Å $\rightarrow 1$. The SCBA approximation gives $\beta \approx 2.2 \approx 300$ meV.

The effective mass corresponding to this value is approximately twice the electron mass, and this agrees with recent measurement of Shubnikov–de Haas oscillations.[40] In the present work, we use β as a fitting parameter. We will see that to fit inelastic neutron data at $x=0.1$, we need

$$\beta \approx 2.7. \tag{3}$$

This agrees well with the value obtained within the SCBA. The quasiparticle residue Z at the minimum of the dispersion is $Z\approx 0.38$.[32] In the full-pocket description, where two half-pockets are shifted by the AF vector $\mathbf{Q}_{AF}=(\pi,\pi)$, the two minima are located at $S_a=(\frac{\pi}{2},\frac{\pi}{2})$ and $S_b=(\frac{\pi}{2},-\frac{\pi}{2})$. The system is thus somewhat similar to a two-valley semiconductor.

The relevant energy scale for small uniform doping at zero temperature is of the order of $xJ \ll J$, relevant momenta are also small, $q \ll 1$. Hence, one can simplify the Hamiltonian of the t-J model by integrating out all high-energy fluctuations. This procedure leads to the effective Lagrangian or effective action. The effective Lagrangian has been first discussed quite some time ago,[26,42,43] see also a recent work.[44] That discussion resulted in the kinematic structure of the effective Lagrangian valid in the static limit.[26] This limit is sufficient only for the mean-field approximation. The time-dependent terms that are necessary for excitations and quantum fluctuations have been derived only recently.[39] The effective Lagrangian can be written in terms of the bosonic $\vec{n}$ field that describes the staggered component of the copper spins and in terms of fermionic holons ψ. We use the term "holon" instead of "hole" because spin and charge are to some extent separated, see discussion below. The holon has a pseudospin that originates from two sublattices, so the fermionic field ψ is a spinor acting on pseudospin. For the hole-doped case, the effective Lagrangian reads

$$\mathcal{L} = \frac{\chi_\perp}{2}\dot{\vec{n}}^2 - \frac{\rho_s}{2}(\nabla\vec{n})^2 + \sum_\alpha \Big\{ \frac{i}{2}[\psi_\alpha^\dagger \mathcal{D}_t\psi_\alpha - (\mathcal{D}_t\psi_\alpha)^\dagger\psi_\alpha] - \psi_\alpha^\dagger\epsilon_\alpha(\mathcal{P})\psi_\alpha + \sqrt{2}g(\psi_\alpha^\dagger\vec{\sigma}\psi_\alpha)\cdot[\vec{n}\times(\mathbf{e}_\alpha\cdot\nabla)\vec{n}]\Big\}. \tag{4}$$

The first two terms in the Lagrangian represent the usual nonlinear σ model, the field $\vec{n}$ is the subject of the constraint $n^2=1$. The magnetic susceptibility and the spin stiffness are $\chi_\perp \approx 0.53/8 \approx 0.066$ and $\rho_s \approx 0.18$.[45] These values are slightly different from that found in Ref. 46. We use the most recent result,[45] see also comment.[47] Note that ρ_s is the bare spin stiffness, therefore by definition, it is independent of doping. It is pointless to introduce a renormalized effective spin stiffness that depends on doping. The excitation spectrum cannot be described by an effective stiffness.

The rest of the Lagrangian in Eq. (4) represents the fermionic holon field and its interaction with the $\vec{n}$ field. The coupling constant is,[28] $g \approx Zt \approx 1$. The index $\alpha = a, b$ (flavor) indicates the location of the holon in momentum space (either in pocket S_a or S_b). The kinematic structure of the coupling term was first derived in Ref. 26. The operator $\vec{\sigma}$ is a pseudospin that originates from the existence of two sublattices, and $\mathbf{e}_\alpha = (1/\sqrt{2}, \pm 1/\sqrt{2})$ is a unit vector orthogonal to the face of the magnetic Brillouin zone (MBZ) where the holon is located. Kinetic energy of the holon, $\epsilon_\alpha(\mathbf{p})$, is quadratic in the momentum $\mathbf{p}$ and generally speaking, it can be anisotropic. However, in LSCO, the anisotropy is small and we use the isotropic approximation [Eq. (2)].

A very important point is that the argument of ϵ in Eq. (4) is a "long" (covariant) momentum,[26]

$$\mathcal{P} = -i\,\boldsymbol{\nabla} + \frac{1}{2}\vec{\sigma}\cdot[\vec{n}\times\boldsymbol{\nabla}\vec{n}]. \tag{5}$$

An even more important point is that the time derivatives that stay in the kinetic energy of the fermionic field are also long (covariant),[39]

$$\mathcal{D}_t = \partial_t + \frac{i}{2}\vec{\sigma}\cdot[\vec{n}\times\dot{\vec{n}}]. \tag{6}$$

The covariant time derivatives result in the "Berry phase term,"[39] $-\frac{1}{2}\psi_\alpha^\dagger\vec{\sigma}\psi_\alpha\cdot[\vec{n}\times\dot{\vec{n}}]$, that is crucially important for excitation spectrum and hence for stability of the system with respect to quantum fluctuations.

Generally speaking, there are also quartic in fermion operators terms in the effective Lagrangian. However, these terms are not important at low doping and therefore we disregard them in Eq. (4).

The effective Lagrangian (4) is valid regardless if the $\vec{n}$ field is static or dynamic. In other words, it does not matter if the ground-state expectation value of the staggered field is nonzero, $\langle\vec{n}\rangle \neq 0$, or zero, $\langle\vec{n}\rangle = 0$. The only condition for validity of Eq. (4) is that all dynamic fluctuations of the $\vec{n}$ field are slow, $1/\tau \ll J$, where τ is the typical time scale of the fluctuations. We will demonstrate below that the dimensionless parameter

$$\lambda = \frac{2g^2}{\pi\beta\rho_s} \tag{7}$$

plays an important role in the theory. If $\lambda \leq 1$, the ground state corresponding to the Lagrangian (4) is the collinear Néel state and it stays collinear at any small doping. If $1 \leq \lambda \leq 2$, the Néel state is unstable at arbitrary small doping and the ground state is static or dynamic spin spiral. Whether the spin spiral is static or dynamic depends on doping. If $\lambda \geq 2$, the system is unstable with respect to phase separation, and hence the effective long-wavelength Lagrangian (4) is meaningless. Thus,

$$\lambda \leq 1, \quad \text{Neel state}$$

$$1 \leq \lambda \leq 2, \quad \text{Spiral state, static or dynamic}$$

$$\lambda \geq 2, \quad \text{Phase separation}. \tag{8}$$

For LSCO the value is $\lambda \approx 1.3-1.5$.

We would like to stress once more that spin and charge to some extent are separated in the effective low-energy Lagrangian (4), this is why we use the term holon instead of hole. The holon carries pseudospin, it carries charge, but it does not carry spin in the usual sense. However, it is not the full spin-charge separation like in one-dimensional (1D) models. To illustrate this point, it is instructive to look at the holon interaction with uniform external magnetic field.[37,39]

$$\delta\mathcal{L}_B = \frac{1}{2}(\vec{B}\cdot\vec{n})\psi_\alpha^\dagger(\vec{\sigma}\cdot\vec{n})\psi_\alpha. \tag{9}$$

Since we only want to stress the spin dynamics, this interaction does not include terms that originate from the long derivative with respect to magnetic vector potential $-i\boldsymbol{\nabla} \to -i\boldsymbol{\nabla} - \frac{e}{c}\mathbf{A}$, describing the interaction of the magnetic field with the electric charge. Clearly the interaction [Eq. (9)] is quite unusual and this is what we call "the partial spin-charge separation." The holon does not interact directly with the staggered magnetic field (neutron scattering).

III. CRITERION OF STABILITY OF THE NÉEL PHASE UNDER DOPING

One can consider the coupling constant g in the Lagrangian (4) as a formal parameter. It is clear that the Néel order must be stable at a sufficiently small g,

$$\vec{n} \approx \vec{n}_0 = (0,0,1). \tag{10}$$

In this case, the two hole pockets are populated by holons with pseudospin "up" and "down," and hence the Fermi momentum (radius of the pocket) is

$$p_F = \sqrt{\pi x}, \tag{11}$$

where x is doping. The Lagrangian (4) can be split in the diagonal and off-diagonal part with respect to transverse spin waves $n_\perp = n_\pm = (n_x \pm i n_y)/\sqrt{2}$.

$$\mathcal{L} = \mathcal{L}_0 + \mathcal{L}_1,$$

$$\mathcal{L}_0 = \frac{\chi_\perp}{2}\dot{n}_\perp^2 - \frac{\rho_s}{2}\left(1 + \frac{\beta x}{4\rho_s}\right)(\boldsymbol{\nabla} n_\perp)^2 + \sum_\alpha \left(\frac{i}{2}[\psi_\alpha^\dagger\dot{\psi}_\alpha - \dot{\psi}_\alpha^\dagger\psi_\alpha] - \psi_\alpha^\dagger\epsilon(\mathbf{p})\psi_\alpha\right),$$

$$\mathcal{L}_1 = \sum_\alpha \psi_\alpha^\dagger\left(-\frac{1}{2}\vec{n}_0[\dot{\vec{n}}_\perp\times\vec{\sigma}] - \frac{\beta}{4}\{\mathbf{p}, \vec{n}_0[\partial\vec{n}_\perp\times\vec{\sigma}]\} + \sqrt{2}g\vec{n}_0[(\mathbf{e}_\alpha\cdot\boldsymbol{\nabla}\vec{n}_\perp)\times\vec{\sigma}]\right)\psi_\alpha. \tag{12}$$

Here, $\{\ldots,\ldots\}$ stands for the anticommutator. Using the second quantization representation for the $\vec{n}$ field,

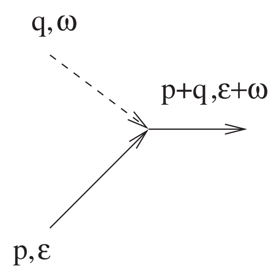

FIG. 1. Magnon-holon vertex, magnon is shown by the dashed line

$$n_{\pm}=\sum_{\mathbf{q}}\frac{1}{\sqrt{2\chi_{\perp}\omega_{\mathbf{q}}}}(e^{i\omega_{\mathbf{q}}t-i\mathbf{q}\cdot\mathbf{r}}m^{\dagger}_{\pm,\mathbf{q}}+e^{-i\omega_{\mathbf{q}}t+i\mathbf{q}\cdot\mathbf{r}}m_{\pm,\mathbf{q}}),$$

with the magnon creation and annihilation operators $m^{\dagger}_{\pm,\mathbf{q}}$ and $m_{\pm,\mathbf{q}}$, we find the "bare" magnon dispersion

$$\omega_{\mathbf{q}}^2=c^2q^2\left(1+\frac{\beta x}{4\rho_s}\right),\quad c^2=\frac{\rho_s}{\chi_{\perp}}, \tag{13}$$

and the pseudospin-flip magnon-holon vertex M shown in Fig. 1,

$$M=i\sqrt{\frac{2}{\chi_{\perp}}}\left\{\sqrt{2}g(\mathbf{e}_{\alpha}\cdot\mathbf{q})+\frac{\omega}{2}+\frac{1}{2}[\epsilon(\mathbf{p})-\epsilon(\mathbf{p}+\mathbf{q})]\right\}. \tag{14}$$

Looking at Eq. (13), one can conclude superficially that magnons are hardened by doping. However, they are not hardened, they are softened. To see this, we need to calculate the magnon polarization operator that is due to $\mathcal{L}_1$. The operator reads

$$\begin{aligned}\mathcal{P}_N(\omega,\mathbf{q})=&\frac{2}{\chi_{\perp}}\sum_{\mathbf{p},\alpha}f_{\mathbf{p}}(1-f_{\mathbf{p+q}})\frac{\left\{\sqrt{2}g(\mathbf{e}_{\alpha}\cdot\mathbf{q})+\frac{\omega}{2}+\frac{1}{2}[\epsilon(\mathbf{p})-\epsilon(\mathbf{p}+\mathbf{q})]\right\}^2}{\epsilon(\mathbf{p})+\omega-\epsilon(\mathbf{p}+\mathbf{q})+i0}\\&+\frac{2}{\chi_{\perp}}\sum_{\mathbf{p},\alpha}f_{\mathbf{p}}(1-f_{\mathbf{p-q}})\frac{\left\{\sqrt{2}g(\mathbf{e}_{\alpha}\cdot\mathbf{q})+\frac{\omega}{2}+\frac{1}{2}[\epsilon(\mathbf{p}-\mathbf{q})-\epsilon(\mathbf{p})]\right\}^2}{\epsilon(\mathbf{p})-\omega-\epsilon(\mathbf{p}-\mathbf{q})+i0},\end{aligned} \tag{15}$$

where $f_{\mathbf{p}}$ is the usual Fermi-Dirac step function. Equation (15) can be transformed to

$$\mathcal{P}_N(\omega,\mathbf{q})=-\frac{\beta c^2x}{4\rho_s}q^2+2\mathcal{P}_0(\omega,\mathbf{q}),$$

$$\mathcal{P}_0(\omega,\mathbf{q})=\frac{2c^2g^2}{\rho_s}q^2\sum_{\mathbf{p}}f_{\mathbf{p}}(1-f_{\mathbf{p+q}})\left(\frac{1}{\epsilon(\mathbf{p})+\omega-\epsilon(\mathbf{p}+\mathbf{q})+i0}+\frac{1}{\epsilon(\mathbf{p})-\omega-\epsilon(\mathbf{p}+\mathbf{q})+i0}\right). \tag{16}$$

An explicit expression for the polarization operator P_0 reads

$$\begin{aligned}\mathrm{Re}\,\mathcal{P}_0(\omega,q)=&-\frac{c^2g^2}{\pi\beta^2\rho_s}\{\beta q^2-R_1\sqrt{1-R_0^2/R_1^2}\theta(1-R_0^2/R_1^2)\\&-R_2\sqrt{1-R_0^2/R_2^2}\theta(1-R_0^2/R_2^2)\},\end{aligned}$$

$$\begin{aligned}\mathrm{Im}\,\mathcal{P}_0(\omega,q)=&-\frac{c^2g^2}{\pi\beta^2\rho_s}\{\theta(R_0^2-R_1^2)\sqrt{R_0^2-R_1^2}\\&-\sqrt{R_0^2-R_2^2}\theta(R_0^2-R_2^2)\},\end{aligned}$$

$$R_0=\beta qp_F,\quad R_1=\frac{1}{2}\beta q^2-\omega,\quad R_2=\frac{1}{2}\beta q^2+\omega. \tag{17}$$

The Fermi momentum p_F is given by Eq. (11), and $\theta(x)$ is the usual step function. With account of the polarization, the magnon Green's function is of the following form:

$$G=\frac{\chi_{\perp}^{-1}}{\omega^2-\omega_{\mathbf{q}}^2-\mathcal{P}_N(\omega,\mathbf{q})+i0}=\frac{\chi_{\perp}^{-1}}{\omega^2-c^2q^2-2\mathcal{P}_0(\omega,\mathbf{q})+i0}. \tag{18}$$

The condition of stability of the ground state is the absence of poles of the Green's function at imaginary ω axis. Hence, this condition is $c^2q^2\geq-2\mathcal{P}_0(0,\mathbf{q})=\lambda c^2q^2$, at $q\ll p_F$. Doping x does not appear in this criterion. Thus, as it is stated in Eq. (8), the Néel state is stable at small doping if $\lambda\leq 1$, and it is unstable at arbitrary small doping if $\lambda\geq 1$. The instability criterion was first derived in Ref. 48 and then discussed many times, see e.g., Refs. 30 and 32. We have rederived it here just to demonstrate how the effective action technique works in the known situation.

IV. THE SPIRAL GROUND STATE IN THE MEAN-FIELD APPROXIMATION

At $\lambda\geq 1$, the minimum energy is realized with the coplanar spiral

$$\vec{n}_0=(\cos\mathbf{Q}\cdot\mathbf{r},\ \sin\mathbf{Q}\cdot\mathbf{r},\ 0), \tag{19}$$

where $\mathbf{Q}\propto(1,0);(0,1)$ is directed along the Cu–O bond. To be specific, we assume that $\mathbf{Q}\propto(1,0)$. Due to the holon interaction with the spiral, the holon band is split in two with $\sigma_z=\pm 1$,

$$\epsilon \to -\frac{\Delta}{2}\sigma_z + \frac{1}{2}\beta\left(\mathbf{p} + \frac{1}{2}\mathbf{Q}\sigma_z\right)^2,$$

$$\Delta = 2gQ. \tag{20}$$

In the ground state, only the band with $\sigma_z = +1$ is populated. Therefore, the Fermi momentum, that is the radius of the Fermi circle in each pocket, is

$$p_F = \sqrt{2\pi x}. \tag{21}$$

The point $\mathbf{p}=0$ corresponds to $\mathbf{k}=(\pi/2, \pm\pi/2)$ in the Brillouin zone. According to Eq. (20), the center of the filled holon pocket ($\sigma_z=1$) is shifted from this point by $-\frac{1}{2}\mathbf{Q}$, and the center of the empty pocket ($\sigma_z=-1$) is shifted by $\frac{1}{2}\mathbf{Q}$. Calculation of energy and its minimization with respect to Q gives the following value:

$$Q = \frac{g}{\rho_s}x. \tag{22}$$

The ground state energy of the spiral state is below that of the Néel state only if $\lambda \geq 1$.

V. THE IN-PLANE MAGNONS IN THE SPIRAL STATE

To analyze the stability of the spiral state, one needs to go beyond the mean-field approximation and study excitations and quantum fluctuations in the system. In this section, we consider in-plane magnetic excitations. An in-plane excitation is described by a small deviation $\varphi = \varphi(t, \mathbf{r})$ from the uniform spiral ground state [Eq. (19)],

$$\vec{n} = [\cos(\mathbf{Q}\cdot r + \varphi), \sin(\mathbf{Q}\cdot r + \varphi), 0]. \tag{23}$$

In the ground state, all the holons are in the pseudospin state $\sigma_z=1$. The in-plane magnons do not change pseudospin; therefore, in this section, we set everywhere $\sigma_z=1$. Substituting expression (23) in the Lagrangian (4), we once more find the diagonal and off-diagonal parts of the Lagrangian

$$\mathcal{L} = \mathcal{L}_0 + \mathcal{L}_1,$$

$$\mathcal{L}_0 = \frac{\chi_\perp}{2}\dot{\varphi}^2 - \frac{\rho_s}{2}\left(1 + \frac{\beta x}{4\rho_s}\right)(\boldsymbol{\nabla}\varphi)^2 + \sum_\alpha \left(\frac{i}{2}[\psi_\alpha^\dagger\dot{\psi}_\alpha - \dot{\psi}_\alpha^\dagger\psi_\alpha] - \psi_\alpha^\dagger\left[-\frac{\Delta}{2} + \epsilon(\mathbf{l}^2)\right]\psi_\alpha\right),$$

$$\mathcal{L}_1 = \sum_\alpha \psi_\alpha^\dagger\psi_\alpha\left(\sqrt{2}g(\mathbf{e}_\alpha\cdot\boldsymbol{\nabla})\varphi - \frac{1}{2}\dot{\varphi} - \frac{\beta}{4}\{\boldsymbol{l}, \partial\varphi\}\right). \tag{24}$$

Here, $\mathbf{l} = \mathbf{p} + \mathbf{Q}/2$ is shifted momentum and $\{\ldots,\ldots\}$ stands for anticommutator. Thus, the bare magnon dispersion is given by the same Eq. (13) as for the Néel state, but the magnon-holon vertex is smaller than Eq. (14) by the factor $\sqrt{2}$,

$$M = i\sqrt{\frac{1}{\chi_\perp}}\left\{\sqrt{2}g(\mathbf{e}_\alpha\cdot\mathbf{q}) + \frac{\omega}{2} + \frac{1}{2}[\epsilon(\mathbf{l}) - \epsilon(\mathbf{l}+\mathbf{q})]\right\}. \tag{25}$$

A calculation similar to that performed in Sec. III for the Néel state gives the following Green's function for the field φ that describes the in-plane magnon:

$$G_{\text{in}} = \frac{\chi_\perp^{-1}}{\omega^2 - c^2q^2 - \mathcal{P}_0 + i0}, \tag{26}$$

where $\mathcal{P}_0$ is given by Eqs. (16) and (17) with the Fermi momentum determined by Eq. (21). At zero frequency and at small q, $q \ll p_F$, the polarization operator is equal to $\mathcal{P}_0(0,\mathbf{q}) = -\frac{\lambda}{2}c^2q^2$. Therefore, the ground state is getting unstable (poles of the Green's function at imaginary ω axis) at $\lambda \geq 2$. This is the instability with respect to charge density wave (CDW) or phase separation[30,32] and it is fatal for the effective long-wavelength Lagrangian (4). Thus, the spiral state is stable at $1 \leq \lambda \leq 2$, see Eq. (8).

It is convenient to define the magnon spectral density as

$$I_{\text{in}}(\omega,\mathbf{q}) = -4\rho_s \,\text{Im}\, G_{\text{in}}(\omega, q). \tag{27}$$

Plots of $2\omega I_{\text{in}}(\omega,\mathbf{q})$ versus ω are presented in Fig. 2(a) for different values of momentum q (offsets). The doping is $x=0.1$, and $\beta=2.7$, $g=1$. The narrow peak is the δ function broadened "by hands" to fit in the picture size. The corresponding quasiparticle residue is rather small, say for $q=0.1Q$ in Fig. 2(a), the residue is $Z=0.39$ and it very quickly dies out at larger values of q. The magnon "dissolves" in the particle-hole continuum.

The q-integrated in-plane magnon spectral density

$$I_{\text{in}}(\omega) = \int I_{\text{in}}(\omega,\mathbf{q})\frac{d^2q}{(2\pi)^2} \tag{28}$$

is plotted in Fig. 2(b) for doping $x=0.025$, $x=0.05$, and $x=0.1$. For zero energy the value of the q-integrated spectral density is independent of doping and equals to $I_{\text{in}}(0)=1/(1-\lambda/2)$.

To calculate the in-plane spectral density that can be observed in neutron scattering, one needs to shift momenta. The Hamiltonian describing the interaction of the neutron spin $\vec{S}^N$ with the $\vec{n}$ field reads

$$H^N \propto \vec{S}^N\cdot\vec{n} = S_z^N n_z + \frac{1}{2}(S_+^N n_- + S_-^N n_+). \tag{29}$$

After the substitution of the in-plane excitation [Eq. (23)], the above Hamiltonian reads

$$H^N \propto \frac{1}{2}S_+^N e^{-i(\mathbf{Q}\cdot\mathbf{r}+\varphi)} + \frac{1}{2}S_-^N e^{i(\mathbf{Q}\cdot\mathbf{r}+\varphi)} \to \frac{1}{2}e^{i\mathbf{k}\cdot\mathbf{r}}\{S_+^N e^{-i\mathbf{Q}\cdot\mathbf{r}}(1-i\varphi) + S_-^N e^{i\mathbf{Q}\cdot\mathbf{r}}(1+i\varphi)\},$$

where $\mathbf{k}$ is the momentum transfer and $\mathbf{Q}$ the momentum shift due to the spiral ground state. The scattering probability for unpolarized neutrons is given by

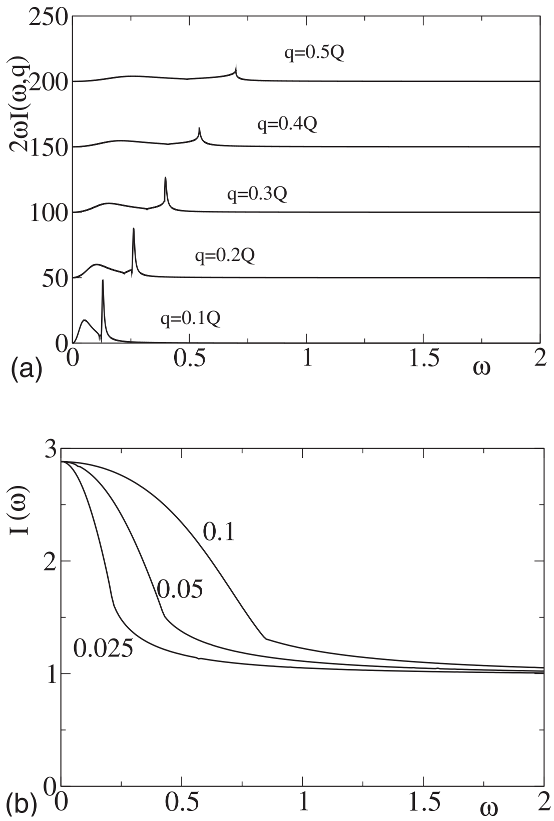

FIG. 2. (a) Plots of $2\omega I_{\text{in}}(\omega,q)$ versus energy for different values of momentum q (offsets). $I_{\text{in}}(\omega,q)$ is the in-plane magnon spectral density [Eq. (27)]. The plots are presented for doping $x=0.1$, and $\beta=2.7$, $g=1$. Values of q are given in units of the incommensurate vector Q, see Eq. (22). (b) q-integrated in-plane spectral density [Eq. (28)] for dopings $x=0.025$, 0.05, and 0.1. The parameters of the effective Lagrangian are $\beta=2.7$, $g=1$.

$$\mathcal{I}_{\text{in}}(\omega,\mathbf{k}) = \frac{1}{2}[I_{\text{in}}(\omega,\mathbf{k}-\mathbf{Q}) + I_{\text{in}}(\omega,\mathbf{k}+\mathbf{Q})]. \tag{30}$$

In Fig. 3, we show by dotted lines the brunches of linear dispersion that correspond to the quasiparticle peak in the spectral function $I_{\text{in}}(\omega,\mathbf{q})$ plotted in Fig. 2(a). The dispersion is very steep, steeper than the bare magnon velocity c, and the corresponding intensities are very low.

VI. THE OUT-OF-PLANE MAGNONS IN THE SPIRAL STATE

Dynamics of out-of-plane magnons are the most complicated ones. Stability of the spiral state was questioned because of the "marginal" character of the out-of-plane excitations if considered in semiclassical $1/S$ approximation.[26,30] The effective action technique allows us to resolve the problem because the technique accounts exactly all the symmetries.

For the out-of-plane excitation let us write the $\vec{n}$ field as

$$\vec{n} = (\sqrt{1-n_z^2}\cos\mathbf{Q}\cdot\mathbf{r}, \sqrt{1-n_z^2}\sin\mathbf{Q}\cdot\mathbf{r}, n_z),$$

and substitute this expression into the effective Lagrangian (4). Neglecting cubic and higher order terms in n_z, we get the

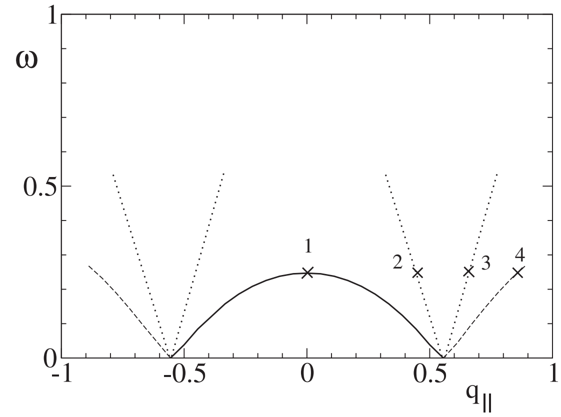

FIG. 3. The magnon dispersion along $\mathbf{Q}$. The parameters are $x=0.1$, $\beta=2.7$, $g=1$. The out-of-plane excitation for $|q|\leq Q$ is shown by the solid line and the out-of-plane excitation for $|q|\geq Q$ is shown by the dashed line. The in-plane excitation is shown by the dotted line. The quasiparticle residue decays very quickly outside of the dome shown by the solid line. The quasiparticle residue at point 1 at the top of the dome is $Z=0.8$ while the quasiparticle residue at point 4 that is outside of the dome at the same height is just $Z=0.13$. The quasiparticle residue of the in-plane magnon at the same frequency as the dome height (points 2 and 3) is $Z=0.15$.

diagonal and the off-diagonal parts of the Lagrangian

$$\mathcal{L} = \mathcal{L}_0 + \mathcal{L}_1,$$

$$\mathcal{L}_0 = \frac{\chi_\perp}{2}\dot{n}_z^2 - \frac{\rho_s}{2}\left(1+\frac{\beta x}{4\rho_s}\right)[Q^2 n_z^2 + (\nabla n_z)^2] + \sum_\alpha\left(\frac{i}{2}[\psi_\alpha^\dagger\dot{\psi}_\alpha - \dot{\psi}_\alpha^\dagger\psi_\alpha] - \psi_\alpha^\dagger\left[-\frac{\Delta}{2}\sigma_z + \frac{\beta}{2}\left(\mathbf{p}+\frac{1}{2}\mathbf{Q}\sigma_z\right)^2\right]\psi_\alpha\right),$$

$$\mathcal{L}_1 = -\sum_\alpha \psi_\alpha^\dagger\frac{\sigma_+}{2}\left(e^{-i\mathbf{Q}\cdot\mathbf{r}}\left[g[Qn_z - i\sqrt{2}(\mathbf{e}_\alpha\cdot\nabla)n_z] + \frac{i}{2}\dot{n}_z\right] - \frac{\beta}{4}\{\boldsymbol{p}, e^{-i\mathbf{Q}\cdot\mathbf{r}}[\boldsymbol{Q}n_z - i\,\partial\, n_z]\}\right)\psi_\alpha + \text{H.c.} \tag{31}$$

Here, $\sigma_+=\sigma_x+i\sigma_y$ and the bracket $\{\ldots,\ldots\}$ stands for anticommutator. According to Eq. (31), the bare magnon dispersion in this case is

$$\omega_{b,\mathbf{q}}^2 = c^2(Q^2+q^2)\left(1+\frac{\beta x}{4\rho_s}\right). \tag{32}$$

The interaction $\mathcal{L}_1$ generates the following two pseudospin-flip vertexes shown in Fig. 4:

$$M_a = i\sqrt{\frac{1}{\chi_\perp}}\left\{g[Q-\sqrt{2}(\mathbf{e}_\alpha\cdot\mathbf{q})] - \frac{\omega}{2} - \frac{\beta}{4}[(2\mathbf{p}+\mathbf{Q}+\mathbf{q})\cdot(\mathbf{Q}-\mathbf{q})]\right\},$$

$$M_b = i\sqrt{\frac{1}{\chi_\perp}}\left\{ g[Q + \sqrt{2}(\mathbf{e}_\alpha \cdot \mathbf{q})] + \frac{\omega}{2} - \frac{\beta}{4}[(2\mathbf{p} + \mathbf{Q} - \mathbf{q}) \cdot (\mathbf{Q} + \mathbf{q})] \right\}. \tag{33}$$

Hence, the magnon polarization operator determined by the vertexes reads

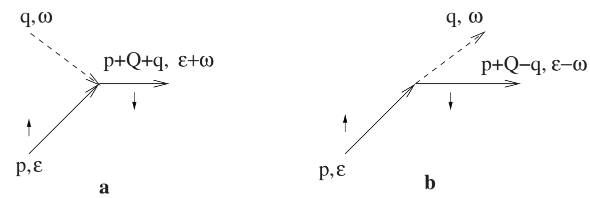

FIG. 4. Magon-holon vertexes with pseudospin flip, magnon is shown by the dashed line.

$$\mathcal{P}(\omega,\mathbf{q}) = \frac{2}{\chi_\perp}\sum_{\mathbf{l}} f_{\mathbf{l}}\left(\frac{\left[g(Q - q_\parallel) - \frac{\omega}{2} - \frac{\beta}{4}(2\mathbf{l} + \mathbf{q}) \cdot (\mathbf{Q} - \mathbf{q})\right]^2 + g^2 q_\perp^2}{\epsilon(\mathbf{l}) - \epsilon(\mathbf{l} + \mathbf{q}) + \omega - \Delta + i0} + \frac{\left[g(Q + q_\parallel) + \frac{\omega}{2} - \frac{\beta}{4}(2\mathbf{l} - \mathbf{q}) \cdot (\mathbf{Q} + \mathbf{q})\right]^2 + g^2 q_\perp^2}{\epsilon(\mathbf{l}) - \epsilon(\mathbf{l} - \mathbf{q}) - \omega - \Delta + i0} \right). \tag{34}$$

Here, $q_\parallel$ and $q_\perp$ are components of momentum parallel and perpendicular to $\mathbf{Q}$, respectively; $f_{\mathbf{l}}$ is the Fermi-Dirac step function and $\mathbf{l}=\mathbf{p}+\mathbf{Q}/2$ is the shifted momentum. Equation (34) can be transformed to

$$\mathcal{P}(\omega,\mathbf{q}) = -\frac{\beta c^2 x}{4\rho_s} q^2 - c^2 Q^2 + \frac{2c^2}{\rho_s}\sum_{\mathbf{l}} f_{\mathbf{l}}\left(\left[g q_\parallel + \frac{\beta}{2}\mathbf{Q} \cdot (\mathbf{l} + \mathbf{q}/2) \right]^2 + g^2 q_\perp^2 \right)\left(\frac{1}{\epsilon(\mathbf{l}) - \omega - \epsilon(\mathbf{l} + \mathbf{q}) - \Delta + i0} + \frac{1}{\epsilon(\mathbf{l}) + \omega - \epsilon(\mathbf{l} + \mathbf{q}) - \Delta + i0} \right). \tag{35}$$

This form is explicitly symmetric with respect to $\omega \to -\omega$ and $\mathbf{q} \to -\mathbf{q}$. Integration in Eq. (35) leads to the following magnon Green's function:

$$G_{\mathrm{out}} = \frac{\chi_\perp^{-1}}{\omega^2 - \omega_{b,\mathbf{q}}^2 - \mathcal{P}(\omega,\mathbf{q}) + i0} = \chi_\perp^{-1}\left[\omega^2 - 2c^2 Q^2 \frac{q_\perp^2}{q^2}\left(1 - \frac{Q^2}{q^2}\right) - c^2 q^2 \left(1 - \frac{Q^2}{q^2}\right)^2 + \frac{c^2}{\pi \beta^2 \rho_s}(F_+ + F_-) + i0 \right]^{-1}, \tag{36}$$

Where

$$\mathrm{Re}\, F_+ = \frac{A}{4q^2} R_\Delta \left[1 - \sqrt{1 - \frac{R_0^2}{R_\Delta^2}}\,\theta\left(1 - \frac{R_0^2}{R_\Delta^2}\right) \right] + \frac{Q^2 q_\perp^2}{6q^6} R_\Delta^3 \left[1 - \sqrt{1 - \frac{R_0^2}{R_\Delta^2}}\left(1 + \frac{R_0^2}{2R_\Delta^2}\right)\theta\left(1 - \frac{R_0^2}{R_\Delta^2}\right) \right],$$

$$\mathrm{Im}\, F_+ = \sqrt{R_0^2 - R_\Delta^2}\,\theta\left(1 - \frac{R_\Delta^2}{R_0^2}\right)\left\{ \frac{A}{4q^2} + \frac{Q^2 q_\perp^2}{6q^6}\left(\frac{R_0^2}{2} + R_\Delta^2\right) \right\},$$

$$A = 4g^2 q^2 + q_\parallel^2 Q^2 \left[\frac{\beta^2}{4} + \frac{2g\beta}{Q} - \frac{R_\Delta}{q^2}\left(\frac{4g}{Q} + \beta\right) \right] + \frac{R_\Delta^2 Q^2}{q^4}(q_\parallel^2 - q_\perp^2),$$

$$R_\Delta = \Delta - \omega + \frac{1}{2}\beta q^2. \tag{37}$$

Here, $\theta(x)$ is the step function and R_0 is defined in Eq. (17). The function F_- is obtained from F_+ by the replacement $\omega \to -\omega$ in R_Δ.

We define the out-of-plane magnon spectral density as

$$I_{\mathrm{out}}(\omega,\mathbf{q}) = -4\rho_s\, \mathrm{Im}\, G_{\mathrm{out}}(\omega,q). \tag{38}$$

Plots of $2\omega I_{\mathrm{out}}(\omega,\mathbf{q})$ versus ω are presented in Fig. 5(a) for different values of momentum $q_\parallel$ (offsets) and $q_\perp=0$. The doping is $x=0.1$. The narrow peak is the δ-function broadened by hands, the effective width is the same as that for in-plane magnons in Fig. 2. The corresponding quasiparticle dispersion $\Omega_{\mathbf{q}}$ is plotted in Fig. 3 for direction along $\mathbf{Q}$, (i.e., $q=q_\parallel$, $q_\perp=0$) and for $x=0.1$. The part for $|q| \le Q$ is shown by the solid line and the part for $|q| \ge Q$ is shown by the dashed line. We do it to stress that the quasiparticle residue decays very quickly outside of the dome. Plot of the residue is shown in Fig. 6(a). To illustrate intensities, we compare points 1–4 in Fig. 3 which correspond to different branches of dispersion with the same frequency. The quasiparticle residue at point 1 at the top of the dome is $Z=0.8$ while the quasiparticle residue at point 4 that is outside of the dome at

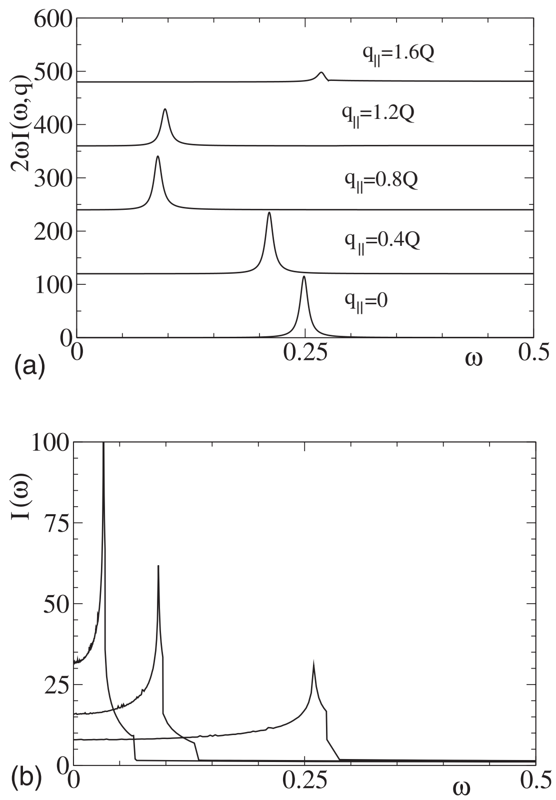

FIG. 5. (a) Plots of $2\omega I_{\text{out}}(\omega,q)$ versus energy for different values of momentum q (offsets). $I_{\text{out}}(\omega,q)$ is the out-of-plane magnon spectral density [Eq. (38)]. The plots are presented for doping $x=0.1$ and $\beta=2.7$, $g=1$. Values of q are given in units of the incommensurate vector Q, see Eq. (22). B: q-integrated out-of-plane spectral density [Eq. (40)] for dopings $x=0.025$, 0.05, and 0.1. The parameters are $\beta=2.7$, $g=1$.

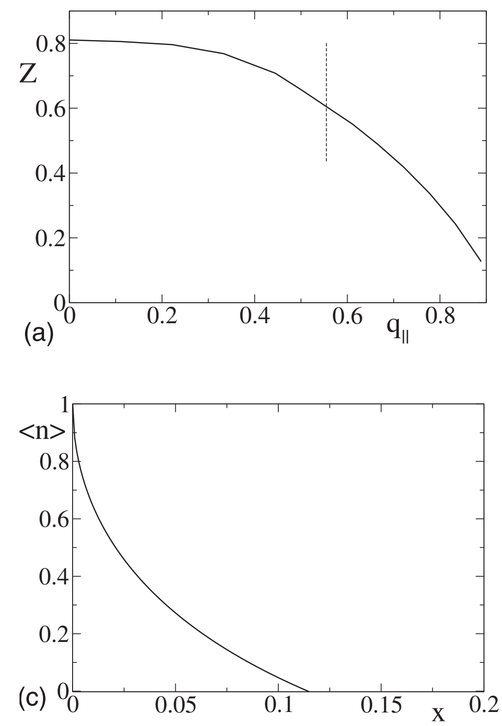

FIG. 6. (a) The quasiparticle residue versus momentum for the out-of-plane magnon for the direction along the spiral, $q=q_{\|}$, $q_{\perp}=0$. The vertical line shows the momentum where the dispersion vanishes. The doping is $x=0.1$. (b) The static component of n field versus doping. The parameters are $g=1$, $\beta=2.7$.

the same height is $Z=0.13$. The quasiparticle residue of the in-plane magnon at the same frequency as the dome height (points 2 and 3 in Fig. 3) is $Z=0.15$.

An analysis of Eq. (36) gives the following approximate formulas for the dispersion of the out-of-plane magnon and for the corresponding quasiparticle residue:

$$\Omega_{\mathbf{q}}^2 \approx \frac{\beta x Q^2 c^2}{4\rho_s}\left(1-\frac{1}{\lambda}\right)\frac{\left(1-\frac{q_{\|}^2}{Q^2}\right)^2+2\frac{q_{\perp}^2}{Q^2}}{1+\frac{c^2q^2}{4g^2Q^2}},$$

$$Z \approx \frac{1}{1+\frac{c^2q^2}{4g^2Q^2}}. \tag{39}$$

These formulas have very limited region of validity since, as we already pointed out, at larger q, the magnon dissolves in the particle-hole continuum. At $x=0.1$, Eq. (39) for $\Omega_{\mathbf{q}}$ agrees reasonably well with the result of numerical calculation shown in Fig. 3. At the same time, the formula (39) for the quasiparticle residue only poorly agrees with numeric shown in Fig. 6(a). Certainly at very small doping, Eq. (39) is accurate.

The q-integrated out-of-plane magnon spectral density

$$I_{\text{out}}(\omega) = \int I_{\text{out}}(\omega,\mathbf{q})\frac{d^2q}{(2\pi)^2} \tag{40}$$

is plotted in Fig. 5(b) for doping $x=0.025$, $x=0.05$, and $x=0.1$. It is peaked at energy E_{cross} corresponding to the top of the dome in Fig. 3. Interestingly, the spectral density decays almost abruptly to its high-frequency asymptotic value $I(\omega)\to 1$ as soon as the magnon is dissolved in the particle-hole continuum. The decay of the in-plane q-integrated spectral density shown in Fig. 2 is not that steep.

VII. QUANTUM FLUCTUATIONS AND QUANTUM PHASE TRANSITION TO THE DYNAMIC SPIRAL PHASE (DIRECTIONAL NEMATIC)

Due to in-plane and out-of plane quantum fluctuations, the static component of the staggered field $\vec{n}$ is reduced,

$$\langle n\rangle \approx 1-\frac{1}{2}\langle\varphi^2\rangle-\frac{1}{2}\langle n_z^2\rangle. \tag{41}$$

Expectation values $\langle\varphi^2\rangle$ and $\langle n_z^2\rangle$ can be expressed in terms of Green's function or in terms of q-integrated spectral densities

$$\langle\varphi^2\rangle = -\sum_{\mathbf{q}}\int\frac{d\omega}{2\pi i}G_{\text{in}}(\omega,\mathbf{q}) = \frac{1}{4\rho_s}\int\frac{d\omega}{2\pi}I_{\text{in}}(\omega),$$

$$\langle n_z^2\rangle = -\sum_{\mathbf{q}}\int \frac{d\omega}{2\pi i}G_{\text{out}}(\omega,\mathbf{q}) = \frac{1}{4\rho_s}\int \frac{d\omega}{2\pi}I_{\text{out}}(\omega). \quad (42)$$

These expressions must be renormalized by subtraction of the ultraviolet-divergent contribution that corresponds to the undoped σ-model. The physical meaning of relations (41) and (42) is very simple: the reduction of static response is transferred to the dynamic response. The most important contribution to quantum fluctuations comes from out-of-plane excitations with momenta $q\sim Q\propto x$. To find this contribution, we use the Green function $G_{\text{out}}\approx \frac{Z_{\mathbf{q}}}{\omega^2-\Omega_{\mathbf{q}}^2}$, where Z and Ω are given by Eq. (39). This gives

$$\langle n_z^2\rangle \to \frac{gc}{\pi^2\sqrt{\beta}\rho_s^{3/2}\sqrt{1-1/\lambda}}B\sqrt{x},$$

$$B = \frac{1}{2}\int_0^\infty\int_0^{\pi/2}\frac{dt d\varphi}{\sqrt{\left(1+\frac{c^2}{4g^2}t\right)[(1-t)^2+2t\cos^2\phi]}}. \quad (43)$$

Thus, the leading term in the quantum fluctuation scales as $\propto\sqrt{x}$. The subleading contribution to the quantum fluctuation scales is x. To find it, we have performed numerical integration in Eq. (42) using q-integrated spectral densities I_{out} and I_{in} calculated in Secs. V and VI, see Fig. 2(b) and Fig. 5(b). This gives

$$\langle n\rangle \approx 1-\frac{gc}{2\pi^2\sqrt{\beta}\rho_s^{3/2}\sqrt{1-1/\lambda}}\mathcal{B}\sqrt{x}+2.6x. \quad (44)$$

Certainly, the coefficient in the subleading x term depends on parameters (a rather weak dependence). The value 2.6 in Eq. (44) corresponds to $g=1$ and $\beta=2.7$. The plot of $\langle n\rangle$ versus doping x at these values of parameters is presented in Fig. 6(b).

According to Fig. 6(b), the static component of $\vec{n}$ vanishes at $x=x_c\approx 0.11$. This is a quantum critical point for transition to the dynamic spiral. In this phase, there is no spontaneous direction of the $\vec{n}$ field, $\langle\vec{n}\rangle=0$, but the spiral direction (1,0) or (0,1) is still spontaneously selected. In our opinion, this is the "nematic phase" observed in Ref. 20. Clearly, the value $x_c\approx 0.11$ is an approximate value. In doing the spin-wave theory, we assume that $\langle\varphi^2\rangle,\langle n_z^2\rangle\ll 1$; but then, to find the critical point, we extend this consideration to $\langle n_z^2\rangle\sim 1$. This extension brings some uncertainty in the value of x_c. We also would like to note that the value of x_c is rather sensitive to parameters. The main sensitivity comes from $\sqrt{1-1/\lambda}$ in the denominator in Eq. (44). The value of λ given by Eq. (7) is closely related to the value of the incommensurate vector Q given by Eq. (22). Our estimate of x_c is valid for LSCO.

At $x\geq x_c$, the spin-wave pseudogap is opened. To describe the gapped phase, we use the Takahashi approach,[49] see also Ref. 50. The idea of this approach is to impose constraint $\langle n\rangle=0$ using the Lagrange multiplier method. So we introduce an additional term in the effective Lagrangian

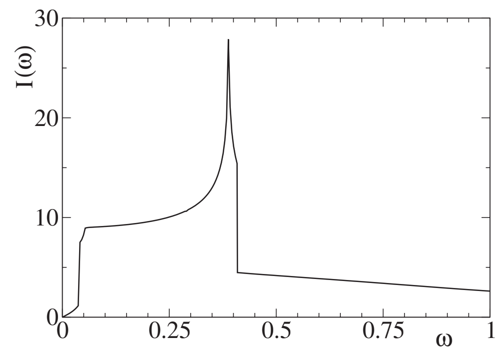

FIG. 7. The q-integrated magnon spectral density $I=I_{\text{in}}+I_{\text{out}}$ in the gapped nematic phase for $x=0.13$ assuming that $x_c=0.11$.

$$\delta\mathcal{L} = \chi_\perp\Delta_s^2\left(1-\frac{1}{2}\varphi^2-\frac{1}{2}n_z^2\right), \quad (45)$$

where Δ_s is technically the Lagrange multiplier, and physically this is the spin-wave pseudogap. The value of Δ_s must be determined from the condition

$$\langle n\rangle = 1-\frac{1}{2}\langle\varphi^2\rangle-\frac{1}{2}\langle n_z^2\rangle = 0. \quad (46)$$

The in-plane quantum fluctuation $\langle\varphi^2\rangle$ is only very weakly (quadratically) dependent on the pseudogap Δ_s. The out-of-plane fluctuation $\langle n_z^2\rangle$ contains a term that depends on Δ_s linearly. The term comes from the $\sqrt{x}$ contribution in Eqs. (43) and (44).

To account for the pseudogap, one needs to replace the expression in square brackets under the square root in B, see Eq. (43), by

$$[(1-t)^2+2t\cos^2\phi]+\frac{4g}{c^2\beta(1-1/\lambda)Q^3}\Delta_s^2. \quad (47)$$

A simple calculation with parameters $g=1$ and $\beta=2.7$ shows that the condition (46) results in the following pseudogap

$$\Delta_s \approx 2.5(x-x_c). \quad (48)$$

This formula is valid only if x is very close to the critical point. In this problem, one cannot expect a high accuracy from the Takahashi-like approach. Therefore, the slope 2.5 in Eq. (48) is rather approximate. Finally, in Fig. 7, we present the plot of the q-integrated magnon spectral density $I_{\text{in}}(\omega)+I_{\text{out}}(\omega)$ for $x=0.13$, assuming that $x_c=0.11$. The figure clearly demonstrates that Δ_s is a pseudogap since there is some spectral weight at $\omega\leq\Delta_s$.

The value of the critical concentration, $x_c\approx 0.11$, agrees well with the available experimental data. According to Ref. 7, quasielastic neutron scattering from LSCO disappears at $x>0.12$. In YBCO, for hole concentration of about 9%, there is still a weak quasielastic scattering,[20] while for hole concentration of about 11%, the quasielastic scattering disappears.[19] Thus in this case, the critical concentration x_c is about 10%. Another confirmation of the critical-point location is the NMR wipeout at low temperature. The wipeout is due to the quasistatic motion of Cu spins. The wipeout exists only at the hole concentration smaller than 0.12–0.13.[51]

TABLE I. LSCO: Experimental values (Ref. 8) of E_{cross} versus doping x.

x	0.025	0.04	0.05	0.07	0.1
E_{cross}(meV)(Ref. 8)	7^{+4}_{-2}	15^{+7}_{-3}	20^{+6}_{-5}	23^{+9}_{-7}	40^{+5}_{-5}
Phase	Insulator			Superconductor	
Spiral direction	Diagonal			Parallel	
Theory	Refs. 38 and 39			Present work	

We would like to note that the pseudogap Δ_s is related to the spin sector only. It is completely unrelated to the pseudogap observed in angular resolved photoemission (ARPES). In our theory, we have the small pocket dispersion [Eq. (2)]. This implies that we are always working in the ARPES pseudogap regime.

According to Eq. (48), the critical index for Δ_s is equal to unity. Certainly, this is only a mean-field result since we use the Takahashi approach. A more accurate calculation of the critical index is an interesting problem. However, the problem is outside of the scope of the present work.

VIII. DISCUSSION AND COMPARISON WITH EXPERIMENT

There are several points that can be directly compared with experiment. The incommensurability vector Q is given by Eq. (22). It depends on the coupling constant g. Fit of experimental incommensurability[7] gives $g\approx 1$ and this agrees remarkably well with prediction of the t-t'-t''-J model.

An important dynamical parameter is E_{cross} which is the height of the dome in Fig. 3. This parameter has been systematically studied very recently in inelastic neutron scattering.[8] The experimental values are presented in Table I. As soon as the coupling constant g is found from the experimental incommensurability Q, we can fit E_{cross}. As we already pointed out above, the present theory is applicable to LSCO at $x \geq x_{per} \approx 0.055$. According to Eq. (39)

$$E_{cross} \approx \sqrt{\frac{\beta x Q^2 c^2}{4\rho_s}\left(1-\frac{1}{\lambda}\right)}. \tag{49}$$

Comparing this formula with data at $x=0.07$ and $x=0.1$ in Table I, we find that $\beta=2.65(1\pm 0.1)$. This value agrees reasonably well with the value $\beta \approx 2.2$ that follows from the t-t'-t''-J model. Note that in principle, the inverse mass β can be somewhat dependent on doping. However, the data with error bars are quite consistent with x-independent β.

Let us also discuss the data at $0.02 \leq x \leq x_{per}=0.055$ that is relevant to the insulating phase with diagonal disordered spin spiral. The corresponding theory has been developed in Refs. 38 and 39. The incommensurability in this case is $Q=\sqrt{2}gx/\rho_s$. To fit the experimental incommensurability, we need $g\approx 0.7$. This is somewhat smaller than the value in the conducting phase. We believe that the reduction of g is due to interaction with phonons. The point is that $g=Zt$, where Z is the quasihole residue. Interaction with phonons in the insulating phase can easily reduce the residue by 20%–30%. Stability of the disordered spiral in the insulating phase is due to localization of holes. The E_{cross} in this case is[39]

$$E_{cross} \approx c\sqrt{\frac{3}{4}\frac{Q^2}{\kappa}}, \tag{50}$$

where κ is the inverse localization length. It is worth noting that Eq. (50) has been derived in Ref. 39 assuming that the binding energy of a hole trapped by Sr ion is larger than the magnon energy. The binding energy is about 10–15 meV. Therefore, strictly speaking, Eq. (50) is applicable only at $x=0.025$ since at larger x the energy E_{cross} is getting too big. Nevertheless, we can try to apply Eq. (50) to the data at $x \leq 0.055$. Fitting the data from Table I, we find values of κ, $x=0.025$: $\kappa=0.55\pm 0.2$, $x=0.04$: $\kappa=0.65\pm 0.2$, and $x=0.05$: $\kappa=0.75\pm 0.2$. So, there is a hint for a weak doping dependence of the inverse localization length κ. Most likely, the dependence is just an imitation of the binding-energy correction to formula (50). On the other hand, a weak dependence of the localization length on doping is quite possible. The above values agree reasonably well with the value $\kappa \approx 0.4$ that follows from the analysis of the variable range hopping conductivity at a very small doping ($x=0.002$), see Ref. 52.

Near $x=0.12$, certain La-based materials in low-temperature tetragonal (LTT) phase develop a strongly enhanced static incommensurate magnetic order accompanied by a small lattice deformation at the second-order harmonics,[9–11] see also Ref. 12 for a review. The measured static magnetic moment $\sim 0.1\ \mu_b$ is substantially larger than the value that follows from the present theory [the unity in the vertical scale in Fig. 6(b) corresponds to the magnetic moment 0.6 μ_B]. There are also experimental indications that the spin structure in this case is close to collinear.[53] We strongly believe that physics of these materials is somehow related to mechanisms considered in the present paper. On the other hand, it is clear that in this case there are some additional effects that are not accounted for by the present theory.

The present theory qualitatively explains the directional nematic state discovered in underdoped YBCO at doping $x \approx 0.09$.[20] For a quantitative comparison, one needs to analyze the two layer situation. This analysis has to include an explanation of a smaller incommensurability compared to that observed in the single-layer LSCO.

In the present work, we did not account for the superconducting pairing. The point is that at *low* doping; the pairing practically does not influence magnetic excitations. From the first sight, this theoretical conclusion is in contradiction with experimental findings.[13,16,19] However, the newest data at very low doping[20] supports this point. Moreover, we believe that a temperature dependence of excitation spectra observed at slightly higher doping[19] is mainly due to the pinning-depinning of the direction of the "electron nematic" rather than due to superconductivity. Our theory is parametrically justified only below the critical concentration x_c and slightly above this concentration. This is the range of doping where the magnetic excitations are independent of the superconducting pairing. Certainly, at a sufficiently low energy, there is still some sensitivity of magnetic spectra to superconductivity. Even in the BCS mechanism phonons with $\omega \sim 2\Delta$ are somewhat sensitive to superconducting pairing. However, this is a sensitivity at the energy scale that is irrelevant to the formation of magnetic excitations. A separate question is how the spiral and the corresponding magnetic excitations influence the superconducting pairing. The spin-wave exchange mechanism for pairing of holons was suggested in Refs. 54 and 55. The mechanism is always working as soon as a short-range antiferromagnetic order exists in the system. So the superconductivity peacefully coexists with spin spirals.[32] Moreover, we understand now that the pairing in the spiral state is strongly enhanced by its closeness to the Néel state instability driven by the parameter λ. The enhancement will be considered elsewhere.

In conclusion, using the low-energy effective field theory, we have considered the 2D t-J model in the limit of small doping. Quantitatively, this consideration is relevant to underdoped single-layer cuprates. We have derived the incommensurate spin structure (static and/or dynamic), calculated spectra of magnetic excitations (Figs. 2, 3, and 5), and considered the quantum phase transition to the directional nematic spin-liquid phase. The spin-wave pseudogap is opened in the spin-liquid phase, the q-integrated spectral density in this case is shown in Fig. 7.

ACKNOWLEDGMENTS

We are very grateful to G. Khaliullin, B. Keimer, J. Sirker and A. Katanin, for valuable discussions. We are also very grateful to B. Keimer and K. Yamada for communicating their results prior to publication. A. I. M. gratefully acknowledges the School of Physics at the University of New South Wales for warm hospitality and financial support during his visit. This work was supported in part by the Australian Research Council.

[1] B. Keimer, A. Aharony, A. Auerbach, R. J. Birgeneau, A. Cassanho, Y. Endoh, R. W. Erwin, M. A. Kastner, and G. Shirane, Phys. Rev. B **45**, 7430 (1992).

[2] M. A. Kastner, R. J. Birgeneau, G. Shirane, and Y. Endoh, Rev. Mod. Phys. **70**, 897 (1998).

[3] M. Matsuda, M. Fujita, K. Yamada, R. J. Birgeneau, Y. Endoh, and G. Shirane, Phys. Rev. B **65**, 134515 (2002).

[4] S. Wakimoto, G. Shirane, Y. Endoh, K. Hirota, S. Ueki, K. Yamada, R. J. Birgeneau, M. A. Kastner, Y. S. Lee, P. M. Gehring, and S. H. Lee, Phys. Rev. B **60**, R769 (1999).

[5] M. Matsuda, M. Fujita, K. Yamada, R. J. Birgeneau, M. A. Kastner, H. Hiraka, Y. Endoh, S. Wakimoto, and G. Shirane, Phys. Rev. B **62**, 9148 (2000).

[6] M. Fujita, K. Yamada, H. Hiraka, P. M. Gehring, S. H. Lee, S. Wakimoto, and G. Shirane, Phys. Rev. B **65**, 064505 (2002).

[7] K. Yamada, C. H. Lee, K. Kurahashi, J. Wada, S. Wakimoto, S. Ueki, H. Kimura, Y. Endoh, S. Hosoya, G. Shirane, R. J. Birgeneau, M. Greven, M. A. Kastner, and Y. J. Kim, Phys. Rev. B **57**, 6165 (1998).

[8] M. Matsuda, M. Fujita, S. Wakimoto, J. A. Fernandez-Baca, J. M. Tranquada, and K. Yamada, arXiv:0801.2254 (unpublished).

[9] J. M. Tranquada, B. J. Sternlieb, J. D. Axe, Y. Nakamura, and S. Uchida, Nature (London) **375**, 561 (1995).

[10] J. M. Tranquada, J. D. Axe, N. Ichikawa, Y. Nakamura, S. Uchida, and B. Nachumi, Phys. Rev. B **54**, 7489 (1996).

[11] M. Fujita, H. Goka, K. Yamada, and M. Matsuda, Phys. Rev. B **66**, 184503 (2002); M. Fujita, H. Goka, K. Yamada, J. M. Tranquada, and L. P. Regnault, *ibid.* **70**, 104517 (2004).

[12] J. M. Tranquada, arXiv:cond-mat/0512115 (unpublished).

[13] P. Bourges, Y. Sidis, H. F. Fong, L. P. Regnault, J. Bossy, A. Ivanov, and B. Keimer, Science **288**, 1234 (2000).

[14] H. F. Fong, P. Bourges, Y. Sidis, L. P. Regnault, J. Bossy, A. Ivanov, D. L. Milius, I. A. Aksay, and B. Keimer, Phys. Rev. B **61**, 14773 (2000).

[15] H. A. Mook, Pengcheng Dai, and F. Dogan, Phys. Rev. Lett. **88**, 097004 (2002).

[16] S. M. Hayden, H. A. Mook, Pengcheng Dai, T. G. Perring, and F. Doğan, Nature (London) **429**, 531 (2004).

[17] V. Hinkov, S. Pailhès, P. Bourges, Y. Sidis, A. Ivanov, A. Kulakov, C. T. Lin, D. P. Chen, C. Bernhard, and B. Keimer, Nature (London) **430**, 650 (2004).

[18] C. Stock, W. J. L. Buyers, Z. Yamani, C. L. Broholm, J.-H. Chung, Z. Tun, R. Liang, D. Bonn, W. N. Hardy, and R. J. Birgeneau, Phys. Rev. B **73**, 100504(R) (2006).

[19] V. Hinkov, P. Bourges, S. Pailhes, Y. Sidis, A. Ivanov, C. D. Frost, T. G. Perring, C. T. Lin, D. P. Chen, and B. Keimer, Nat. Phys. **3**, 780 (2007).

[20] V. Hinkov, D. Haug, B. Fauque, P. Bourges, Y. Sidis, A. Ivanov, C. Bernhard, C. T. Lin, and B. Keimer, Science **319**, 597 (2008).

[21] P. W. Anderson, Science **235**, 1196 (1987).

[22] V. J. Emery, Phys. Rev. Lett. **58**, 2794 (1987).

[23] F. C. Zhang and T. M. Rice, Phys. Rev. B **37**, 3759 (1988).

[24] Y. Tokura, S. Koshihara, T. Arima, H. Takagi, S. Ishibashi, T. Ido, and S. Uchida, Phys. Rev. B **41**, 11657 (1990).

[25] O. K. Andersen, A. I. Liechtenstein, O. Jepsen, and F. Paulsen, J. Phys. Chem. Solids **56**, 1573 (1995); E. Pavarini, I. Dasgupta, T. Saha-Dasgupta, O. Jepsen, and O. K. Andersen, Phys. Rev. Lett. **87**, 047003 (2001).

[26] B. I. Shraiman and E. D. Siggia, Phys. Rev. Lett. **61**, 467 (1988); B. I. Shraiman and E. D. Siggia, *ibid.* **62**, 1564 (1989); B. I.

Shraiman and E. D. Siggia, Phys. Rev. B **42**, 2485 (1990).
[27] T. Dombre, J. Phys. (France) **51**, 847 (1990).
[28] J. I. Igarashi and P. Fulde, Phys. Rev. B **45**, 10419 (1992).
[29] G. C. Psaltakis and N. Papanicolaou, Phys. Rev. B **48**, 456 (1993).
[30] A. V. Chubukov and K. A. Musaelian, Phys. Rev. B **51**, 12605 (1995).
[31] N. Hasselmann, A. H. Castro Neto, and C. M. Smith, Phys. Rev. B **69**, 014424 (2004).
[32] O. P. Sushkov and V. N. Kotov, Phys. Rev. B **70**, 024503 (2004).
[33] V. Juricic, L. Benfatto, A. O. Caldeira, and C. M. Smith, Phys. Rev. Lett. **92**, 137202 (2004).
[34] O. P. Sushkov and V. N. Kotov, Phys. Rev. Lett. **94**, 097005 (2005).
[35] P.-A. Lindgård, Phys. Rev. Lett. **95**, 217001 (2005).
[36] V. Juricic, M. B. Silva Neto, and C. M. Smith, Phys. Rev. Lett. **96**, 077004 (2006).
[37] A. Lüscher, G. Misguich, A. I. Milstein, and O. P. Sushkov, Phys. Rev. B **73**, 085122 (2006).
[38] A. Lüscher, A. I. Milstein, and O. P. Sushkov, Phys. Rev. Lett. **98**, 037001 (2007).
[39] A. Lüscher, A. I. Milstein, and O. P. Sushkov, Phys. Rev. B **75**, 235120 (2007).
[40] N. Doiron-Leyraud, C. Proust, D. LeBoeuf, J. Levallois, J.-B. Bonnemaison, R. Liang, D. A. Bonn, W. N. Hardy, and L. Taillefer, Nature (London) **447**, 565 (2007).
[41] E. Dagotto, Rev. Mod. Phys. **66**, 763 (1994).
[42] P. B. Wiegmann, Phys. Rev. Lett. **60**, 821 (1988).
[43] X. G. Wen, Phys. Rev. B **39**, 7223 (1989).
[44] F. Kampfer, M. Moser, and U.-J. Wiese, Nucl. Phys. B **729**, 317 (2005); C. Brugger, F. Kampfer, M. Moser, M. Pepe, and U.-J. Wiese, Phys. Rev. B **74**, 224432 (2006).
[45] R. R. P. Singh, Phys. Rev. B **39**, 9760 (1989); Zheng Weihong, J. Oitmaa, and C. J. Hamer, *ibid.* **43**, 8321 (1991).
[46] S. Chakravarty, B. I. Halperin, and D. R. Nelson, Phys. Rev. B **39**, 2344 (1989).
[47] In the end the precise value of the spin stiffness is not important. The point is that we determine the value of the coupling constant g by fitting experimental data with Eq. (22). A 20% change in ρ_s would result in the corresponding change of g. We also compare this value of g with that calculated within the t-J model. However, it would be naive to think that the t-J calculation has accuracy better than 20%.
[48] O. P. Sushkov and V. V. Flambaum, Physica C **206**, 269 (1993).
[49] M. Takahashi, Phys. Rev. Lett. **58**, 168 (1987); Phys. Rev. B **40**, 2494 (1989).
[50] P. Chandra, P. Coleman, and A. I. Larkin, J. Phys.: Condens. Matter **2**, 7933 (1990).
[51] M.-H. Julien, A. Campana, A. Rigamonti, P. Carretta, F. Borsa, P. Kuhns, A. P. Reyes, W. G. Moulton, M. Horvatic, C. Berthier, A. Vietkin, and A. Revcolevschi, Phys. Rev. B **63**, 144508 (2001); Y. Kobayashi, T. Miyashita, M. Ambai, T. Fukamachi, and M. Sato, J. Phys. Soc. Jpn. **70**, 1133 (2001).
[52] C. Y. Chen, E. C. Branlund, C. S. Bae, K. Yang, M. A. Kastner, A. Cassanho, and R. J. Birgeneau, Phys. Rev. B **51**, 3671 (1995).
[53] N. B. Christensen, H. M. Ronnow, J. Mesot, R. A. Ewings, N. Momono, M. Oda, M. Ido, M. Enderle, D. F. McMorrow, and A. T. Boothroyd, Phys. Rev. Lett. **98**, 197003 (2007).
[54] V. V. Flambaum, M. Yu. Kuchiev, and O. P. Sushkov, Physica C **227**, 267 (1994).
[55] V. I. Belinicher, A. L. Chernyshev, A. V. Dotsenko, and O. P. Sushkov, Phys. Rev. B **51**, 6076 (1995).